REPORT NO. 46

APRIL, 1951

THE COLLEGE OF AERONAUTICS

CRANFIELD

The Use of a Potential Flow Tank for Testing Axi-Symmetric Contraction Shapes suitable for Wind Tunnels

-by-

A.W. Babister, M.A., A.F.R.Ae.S.
W.S.D. Marshall, D.Ae. (Hull)., A.F.R.Ae.S.,
and
G.M. Lilley, D.I.C.,M.Sc., A.F.R.Ae.S.

of the Department of Aerodynamics

and

E. C. Sills and S. R. Deards

of the Department of Aircraft Design

SUMMARY

The report gives details of tests in the potential flow tank on a series of axi-symmetric contraction shapes. The tests were in connection with the design of the 8ft x 6ft wind tunnel and a water tunnel. The potential flow tank provides a simple method of modifying an axi-symmetric contraction shape to meet given requirements. The report shows that small modifications to a theoretical contraction shape for the 8ft x 6ft wind tunnel give a great reduction in total length with only a small adverse velocity gradient at the high speed end of the contraction. The tests were concerned with contraction ratios of the order of 7:1 , which is considerably larger than the contraction ratio of 4:1 tested by Cheers[2]; thus the electrolyte at the high speed end of the contraction was comparatively shallow, and special care was needed in manufacturing the model and in designing the electronic equipment. Details are given of the precautions taken in consequence. The overall error of the apparatus is ± 2 per cent and suggestions are given for increasing this accuracy.

MEP

LIST OF CONTENTS

NOTATION. (See Figure 1)

ϕ	Velocity or electric Potential
$q = \frac{\partial \phi}{\partial s}$	Velocity at surface of contraction
u_o	Velocity at entry to contraction
μ	Contraction ratio = $\frac{\text{area at entry}}{\text{area at exit}}$
R	Radius at low speed end (AD)
r	Radius at a general point (BE)
x	Distance measured along axis (DE)
s	Distance measured along wall (AB).

/1. Introduction.- ...

1. Introduction

The general technique of measurement in a potential flow tank is now well known, having been described by Malavard[1] and Cheers[2]. A tank has now been set up at the College of Aeronautics and the first major application has been to the design of an axi-symmetric contraction shape for the proposed 8ft x 6ft wind tunnel and to test the design of a water tunnel projected by the Ministry of Works. In these instances we were concerned with contraction ratios of the order of 7:1 , which is considerably larger than the contraction ratio of 4:1 tested by Cheers[2]; thus the electrolyte at the high speed end of the contraction was relatively shallow, and special care had to be exercised in the manufacture of the model, the design of the electronic measuring apparatus, and the overall alignment of the tank. This report gives details of the precautions taken, the sources of possible error, and the overall accuracy of measurement attained.

For the contraction shape required for the 8ft x 6ft tunnel we were able to start with a theoretical shape calculated by Lilley[3] to give a monotonic velocity distribution along any streamline. Such a requirement can only be met theoretically with a shape of infinite length; these tests were designed to see what modifications could be made to the theoretical shape to produce a shape of practical length without incurring an adverse pressure gradient of unacceptable magnitude.

Later tests described in paragraph 4.4 were undertaken at the request of the Ministry of Works in connection with a given contraction shape for a proposed water tunnel. During these tests some improvements were made in the measuring technique enabling the overall error of the apparatus to be assessed.

2. Description of the apparatus

2.1 The tank and probes

Figures 2 and 3 give the general layout of the tank with each of the two probes in use. The tank consists of a heavy wooden frame with a slate bottom. The inside of the tank is lined with glass, the joints being made watertight with 'Bostik'. The whole assembly is supported on an angle iron cradle which permits the tank to be tilted through an angle of $\pm 7^{\circ}$ to the horizontal. The inside dimensions of the tank are 72in x 36in.

/Brass ...

Brass rails are fitted to the sides of the tank. These can be seen in Figures 2 and 3. A trolley, which spans the tank, can run along these rails (Figure 2), and the probe attachment can be moved along the span of the trolley. In levelling the tank and trolley it is necessary to ensure that the rails are parallel to the water line, that the trolley is normal to the rails, and that the movement of the probe attachment is in a horizontal plane. Scales are attached to the rails and the trolley, giving the position of the probe.

Two types of exploring probe are shown in Figures 4 and 5. The standard probe (Figure 4) consists of a short length of platinum wire fixed to a 'Tufnol' plug which is a push fit in a brass tube. At the other end of the brass tube is a screw fitting which attaches the probe to the traversing head. The depth of the probe in the electrolyte is adjusted to be about 0.1in and is then locked.

The wall probe (Figure 5) is the same as the standard probe, except that the platinum wire probe and its insulator are now attached to a metal block which rests on the template surface of the model under test.

As is stated below (paragraph 3.3), the accuracy of the setting of the probe was not as good as was desired, especially with the standard probe. Since these tests were completed, a lathe bed has been mounted alongside the tank and the probe is attached to one arm of the lathe; this enables the probe to be set to within $\pm$ .004in.

2.2 The Electronic Equipment

The arrangement of the electronic equipment is shown in relation to the tank in Figure 6. In effect, it consists of a bridge and a suitable null indicator. The potential at any given point in the tank is determined by comparing this unknown potential detected by the exploring probe with a known potential.

The input signal to the bridge is supplied by a Wein bridge oscillator[4] (270 cycles per sec.). The frequency stability of this oscillator is good, and its wave form reasonably pure. A push-pull power amplifier is added to feed the bridge at 50 volts (root mean square), which voltage is not too high to cause electrolysis and yet is sufficiently high to provide a satisfactory signal/noise ratio. The complete arrangement of the oscillator and power amplifier is given in Figure 7.

/A transformer ...

A transformer, the secondary winding of which is tuned to 270 cycles per sec, couples the out-of-balance signal to the amplifier. A Wagner earth[5] prevents a large potential difference at source frequency appearing between primary and secondary windings of the transformer.

The high impedance of the tank renders the bridge network rather susceptible to extraneous pick-up. This, together with the fact that harmonics of the source generator frequency are also likely to be troublesome, clearly indicates that the amplifier should have a highly selective gain/frequency characteristic with its maximum response at the fundamental frequency of the source generator. Figure 8 gives the circuit of the amplifier employed in these experiments. The selectivity of the amplifier is produced by a 'parallel - T' network. Provision is made to adjust the oscillator frequency to that corresponding to maximum gain of the amplifier. Automatic amplitude control can readily be provided in the Wein bridge oscillator, and this ensures constant amplitude during this adjustment of frequency.

2.3. The Model

To explore the velocity field of an axi-symmetric flow a small sector of the whole is tested in the potential flow tank. In such a test the bottom of the tank is tilted through a small angle (5°). The free water surface and the bottom thus become bounding radii of the sector, and the shore line is the axis of symmetry. Figure 9 shows a typical cross-section through the tank. For accurate representation of the axi-symmetric case the wax surface should not be a straight line but a circular arc with its centre at the shore line. This, however, was too difficult to be practicable and the small error in replacing the circular arc by an equivalent straight chord was accepted.

In setting up a model contraction for test, a plywood template was first mounted in the tank on wooden packing pieces approximately two inches high (see Figure 9). The contraction shape was then rough cast in paraffin wax and finally the wax was hand scraped to the template. It was found that the addition of a little bees' wax to the paraffin wax made the hand scraping much easier. Finally the joint between the glass bottom and the wax contraction shape was made watertight by undercutting the wax for about 3/16inch, as in Figure 9, and packing this undercut with a heavy grease.

/3. Experimental ...

3. Experimental procedure

3.1. General

Tap water was gently poured into the tank until the given contraction ratio was reached. A straight shore line was obtained by using some chemical wetting agent ('Tepol') which was also effective in minimising any surface tension effects.

The correct level of water for a given contraction ratio was determined by measuring the potential gradient at the wall over two sections, one at the highspeed end, the other at the low speed end. Both sections were in the respective parallel portions of the contraction shape. The contraction ratio was determined by the relation

$$\text{Contraction Ratio } \mu = \frac{\frac{\partial \phi}{\partial s} \text{ (high speed)}}{\frac{\partial \phi}{\partial s} \text{ (low speed)}}$$

and the water level was adjusted accordingly until the desired contraction ratio was achieved. This contraction ratio could be verified by measurement of the cross-sectional areas of water at the high and low speed ends. The ratio of the potential gradients gave the more accurate determination of the contraction ratio, as it was difficult to measure lengths accurately under water.

It was essential to ensure that both electrodes were normal to the surface of the contraction, since any off-setting of the electrodes resulted in an apparent curvature of the flow leading to an erroneous velocity gradient along a parallel portion of the contraction.

Other possible sources of error arose from evaporation and from leakage of the water. Once a given test was begun it was essential to complete all the measurements without a long interval between readings. This minimised the change in contraction ratio due to evaporation. Leakage between the wax and the glass was a source of large errors, and could lead to misleading results due to a continuous variation in the contraction ratio while the readings were being taken.

When the water level giving the correct contraction ratio had been determined, measurements of potential ϕ were taken (i) along the wall of the contraction and (ii) in mid-stream at a constant radius r. When the standard

/probe ...

probe and trolley were used, readings were taken at constant intervals of two inches in x (distance measured parallel to the shore line). When the wall probe was used, the wooden template was graduated in constant intervals of 1in. in s (distance along the arc of the contraction shape). Readings of ϕ were taken from within two inches of either electrode. Figure 17 shows that the measured values of $\partial\phi/\partial s$ tend to fall off near the high speed electrode, where the depth of water would be smallest and therefore any meniscus effect on the surface of the electrode would be more important; however, this effect was not noticeable for readings taken at distances greater than $2\frac{1}{2}$ inches from the electrode.

3.2. Determination of the velocity distributions

For a given contraction shape the measured values of the potential ϕ along the wall were replotted against the arc length s as shown in Figure 10. Values of ϕ were then read off at equal intervals of s (every $2\frac{1}{2}$ inches) and the values of the velocity $q = \frac{\partial\phi}{\partial s}$ were found by using Lagrangian five point interpolation coefficients.[6] Finally the ratio of the given velocity q to that at the low speed end u_o was determined and q/u_o was plotted against x as shown in Figures 12-15.

The replotting of the measured value of the potential ϕ in the above analysis inevitably led to some degree of smoothing. To eliminate this, the readings for the water tunnel contraction were taken at constant intervals of s and the values of the velocity were found (i) by taking mean slopes across a double interval (2 inches) and (ii) by Lagrangian interpolation. Figure 17 shows that similar irregularities in the velocity distribution could be detected by both methods.

The velocity in the free stream was determined directly from the readings of ϕ as a function of x, the distances measured parallel to the shore line; in this case there was no need to replot the curve as in the case of the velocity distribution along the wall.

3.3 Accuracy of results

Figure 17 shows the general scatter of points obtained in three tests of the water tunnel contraction under identical conditions. The repeatability of any one reading is approximately $\pm$ 1 per cent during any one test.

/Apart ...

Apart from the sources of errors mentioned in paragraph 3.1, several smaller errors in setting and measurement could be present in the results. The wooden template was cut out to the required contraction shape; the probable error of the dimensions of the template was less than $\pm$ 0.01in. The glass bottom of the tank was not flat. Over the total length of 72in. the glass had a bow of 0.005in., but the error over any 10inch distance was less than 0.001in. When the trolley was used, the setting of the probe could be in error due to

(i) misalignment of the trolley span
(ii) positioning the trolley along the rails
(iii) setting of the probe (e.g. with the standard probe near the wall of the contraction in which the radial distance of the probe would be varying along the contraction).

To minimise these errors, the wall probe was adopted. This could be set to an accuracy of $\pm$ 0.02in.

Throughout the analysis the effect of variation in the depth of probe between high and low speed ends has been neglected. It was found that with a very small depth of probe (say less than 0.05in) it was difficult to obtain good accuracy in the measurement of ϕ.

The electronic apparatus gave the potential ϕ correct to $\pm$ 0.5 per cent.

The probable error due to all these causes at any point was about $\pm$ 2 per cent.

4. Results and Discussion

4.1. Theoretical Contraction

The first contraction shape to be tested in the tank was a theoretical axi-symmetric contraction, contraction ratio 7.0, calculated by Lilley's method[3] to give a monotonic velocity distribution. The ordinates of the contraction are given in Table I and an indication of its shape is shown in Figure 11. The contraction started at $\frac{x}{R} = 0$ and the velocity was within $\frac{1}{2}$ per cent of its final value at $\frac{x}{R} = 5.7$ where $R (= 10\text{in.})$ is the radius of the low speed end. The measured and theoretical velocity distributions at the wall are shown in Figure 12, in which the ratio

$$\frac{q}{u_o} = \frac{\text{local velocity}}{\text{free stream velocity at low speed end}}$$

/is ...

is plotted against $\frac{x}{R}$. The velocity starts to increase at $\frac{x}{R} = 2.5$ and is still increasing slightly at the high speed end; the theoretical velocity distribution tends asymptotically to its final value at infinity.

4.2. Modification to the high speed end

In the design of the 8ft x 6ft wind tunnel, it was essential that the total length of the contraction should not exceed 3.5R (35inches model scale) and that the velocity gradient at the beginning of the working section should be as small as possible. Accordingly, the theoretical contraction was modified at the high speed end from $\frac{x}{R} = 3.7$ onwards, the radii being decreased by up to 0.07in. (see Figure 11). The contraction extended from $\frac{x}{R} = 0$ to $\frac{x}{R} = 4.9$ (a total length of 49 inches). Measurements of the potential ϕ were made both along the wall and in the stream, and the corresponding velocity distributions are given in Figure 13.

The velocity distribution along the wall has a peak at the high speed end, the maximum velocity ratio being 7.4 compared to the final contraction ratio of 7.0, the peak being followed by an adverse pressure gradient. This is in agreement with Goldstein's conclusions[7] for two dimensional channels: that a region of adverse pressure gradient would be found with any contraction of finite length. The velocity peak is associated with the increase in curvature caused by the modification to the high speed end. There is a smaller peak in the velocity distribution in the stream. Both the stream and wall velocity distributions have settled down to the same constant value at $\frac{x}{R} = 5.7$.

4.3. Modifications to the low speed end

To minimise the peak at the high speed end, the low speed end of the contraction was modified so that the beginning of the contraction was at $\frac{x}{R} = 1.6$, the shape running into the previous one at $\frac{x}{R} = 3.7$ (see Figure 11), the radii being increased by up to 0.8in. This modification led to an increase in the curvature at the low speed end following the prolonged parallel portion. This resulted in a trough in the velocity distribution at $\frac{x}{R} = 2.7$ (Figure 13). It will be seen, however, that the modification removed the peak in the wall velocity at the high speed end. The adverse pressure gradient in the low speed region is undesirable as it might lead to a local separation of the boundary layer in the wind tunnel contraction.

/Accordingly ...

Accordingly a further modification was made to the shape at the low speed end. The ordinates for this final contraction shape are given in Table II (and Figure 11); at the low speed end this shape was approximately a mean between those previously tested. The velocity distributions both along the wall and in the stream are shown in Figures 14 and 15. There is now no trough at the low speed end and only a small peak at the high speed end. The total length of the contraction is 3.4 R. The change in velocity distribution takes place in the interval $\frac{x}{R} = 2.0$ to $\frac{x}{R}$ 5.5. This satisfies the conditions imposed by the 8ft x 6ft wind tunnel and this contraction shape was accepted for the tunnel design.

4.4 The water tunnel contraction

In this instance the contraction shape was given and we were asked to comment on it.

The ordinates for this axi-symmetric contraction shape are given in Table III and Figure 16. The contraction ratio is 7.44. The curvature of the shape is rather greater than that predicted by the theoretical work of Lilley for this contraction ratio.

As explained in paragraph 3.3 above, in order to achieve greater accuracy, a wall probe was used in the tests on this shape. The resulting velocity distributions along the surface are given in Figure 17. Three separate tests were made under identical conditions, the second being analysed to obtain the velocity $\frac{\partial \phi}{\partial s}$ (i) by differencing the potential ϕ and (ii) by Lagrangian interpolation. In all the tests there was a tendency to give a double peak at the high speed end. This double peak is smoothed out into a single peak using the Lagrangian interpolation method (the method used in all the previous tests). The overshoot in velocity at the high speed end by 0.6 at least was not considered satisfactory. This may be due to over acceleration in the transition portion accentuated by a larger curvature at the high speed end. From these results it is seen that the proposed contraction shape would not be satisfactory if used in a wind tunnel or water tunnel and would require modification.

/5. Conclusions ...

5. Conclusions

1. From the above results it is concluded that the potential flow tank can be used to provide a simple method of modifying a given axi-symmetric contraction shape. With proper precautions, as described in paragraph 3, the order of error in the wall velocity distribution can be kept within ± 2 per cent.

2. The wall probe gives better accuracy than the standard probe on the moveable trolley since it enables the probe to be set much more accurately. The lathe bed mounting now in use gives much better accuracy than either of the other methods.

3. Other improvements in the apparatus would be obtained by replacing the glass bottom of the tank by either the slate bottom or by a plane surface of wax. The latter would ensure a plane base and give a much better safeguard against leakage.

6. Acknowledgements

Our thanks are due to Vickers Armstrong Ltd., Weybridge, who donated the tank to the College.

The wax models mentioned in this report were made by Mr. G.T. Downer and the wooden templates by Mr. C.D. Bruce.

/References ...

REFERENCES

1. Malavard, L. — The use of rheo-electrical analogies in certain aerodynamical problems. Royal Aeronautical Society Journal Vol. 51, 1947, pp 739-756.

2. Cheers, F. Raymer, W.G. and Fowler, R.G. — Preliminary tests on electric potential flow apparatus. A.R.C. Reports and Memoranda 2205, (1945).

3. Lilley, G.M. — Some theoretical aspects of nozzle design. University of London M.Sc. Thesis, (1945).

4. Terman, F.E. and others — Proceedings Institute of Radio Engineers, Vol. 27, 1939, p.649.

5. Everitt, W.L. — Communication Engineering, 2nd edition. 1937, pp.307-308. McGraw-Hill.

6. Shelley, J.H. — Lagrangian Interpolation Coefficients Using Five Tabulated Values. Gloster Aircraft Company Ltd.

7. Goldstein, S. — Notes on the design of Converging Channels. A.R.C. 8495, F.M. 785, (1945).

/Table I ...

TABLE I

Ordinates for theoretical contraction shape

(Contraction ratio 7/1)

x/R	0	0.2	0.4	0.6	0.8	1.0	1.2
r/R	0.9998	0.9997	0.9995	0.9992	0.9988	0.9980	0.9968
x/R	1.4	1.6	1.8	2.0	2.2	2.4	2.6
r/R	0.9948	0.9915	0.9862	0.9776	0.9636	0.9407	0.9034
x/R	2.8	3.0	3.2	3.4	3.6	3.8	4.0
r/R	0.8446	0.7602	0.6608	0.5689	0.5000	0.4538	0.4246
x/R	4.2	4.4	4.6	4.8	5.0	5.2	5.4
r/R	0.4065	0.3955	0.3887	0.3846	0.3820	0.3805	0.3795
x/R	5.6	5.8	6.0	6.2	6.4	6.6	6.8
r/R	0.3789	0.3786	0.3784	0.3782	0.3781	0.3780_5	0.3780_2
x/R	7.0	7.15					
r/R	0.3780	0.3780					

/Table II ...

TABLE II

Ordinates for final Contraction shape for 8ft x 6ft Wind Tunnel

x/R	0.56	1.76	1.96	2.16	2.36	2.56	2.66
r/R	1.0	1.0	0.996	0.985	0.965	0.940	0.920
x/R	2.76	2.86	2.96	3.06	3.16	3.26	3.36
r/R	0.898	0.867	0.826	0.779	0.726	0.661	0.603
x/R	3.46	3.56	3.66	3.76	3.86	3.96	4.06
r/R	0.555	0.515	0.485	0.461	0.441	0.426	0.414
x/R	4.16	4.26	4.36	4.46	4.56	4.66	4.76
r/R	0.406	0.397	0.391	0.388	0.383_5	0.382	0.380
x/R	4.96	6.76					
r/R	0.378	0.378					

TABLE III

Ordinates for water tunnel Contraction.

x/R	0	0.5	0.7	0.9	1.1	1.3	1.5	1.7	1.9	2.1
r/R	1.0	1.0	0.997	0.994	0.988	0.980	0.969	0.950	0.921	0.882
x/R	2.3	2.5	2.7	2.9	3.1	3.3	3.5	3.7	3.9	
r/R	0.827	0.745	0.621	0.517	0.459	0.424	0.402	0.387	0.377	
x/R	4.1	4.3	4.5	7.2						
r/R	0.372	0.367	0.366	0.366						

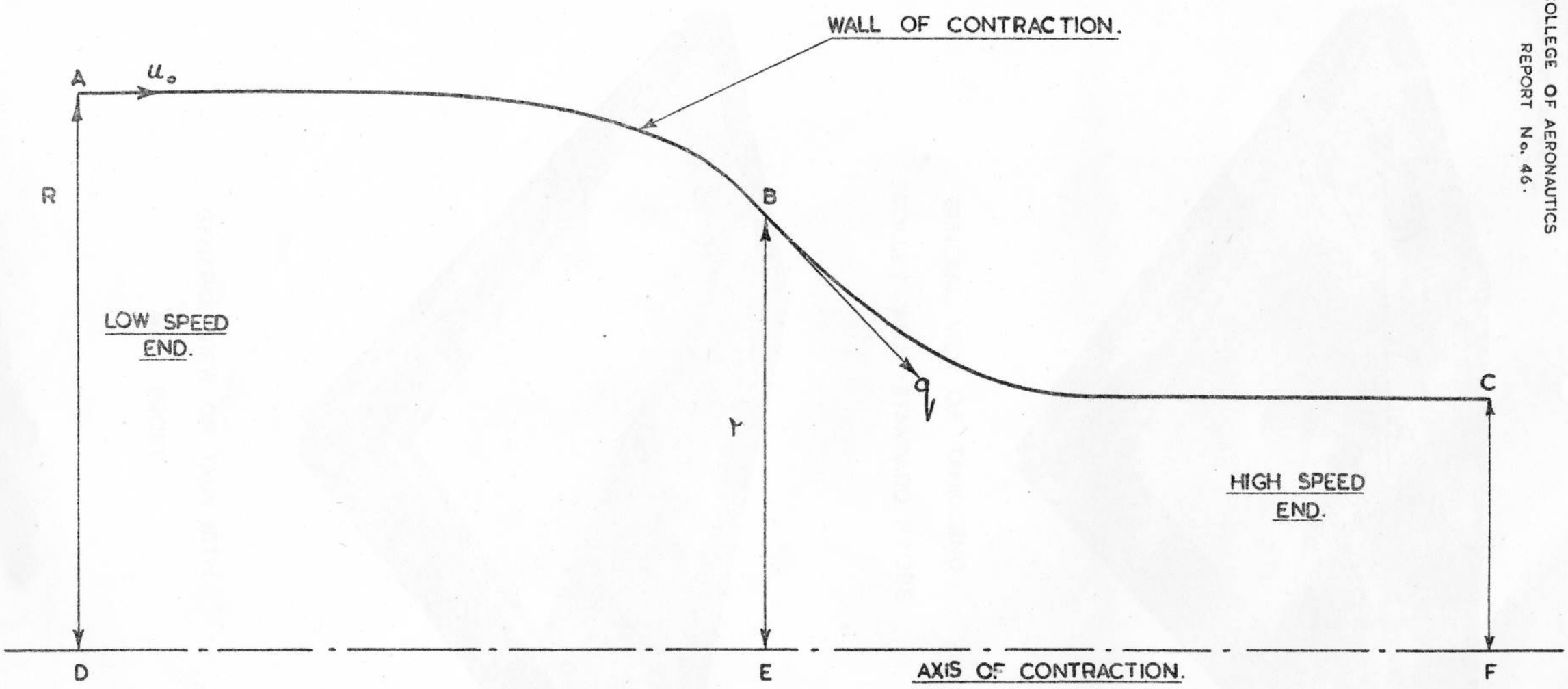

GENERAL DIAGRAM OF CONTRACTION SHAPE.

(NOT DRAWN TO SCALE).

FIG. 1.

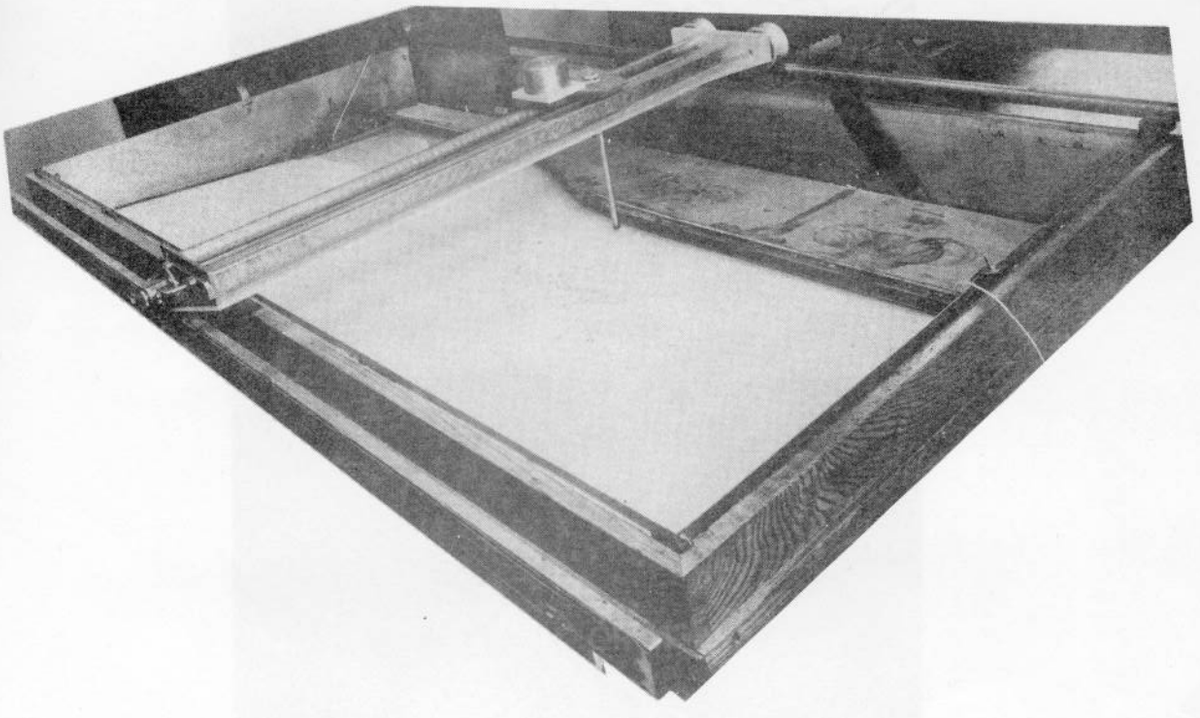

GENERAL VIEW OF TANK AND TROLLEY WITH STANDARD PROBE

FIG. 2

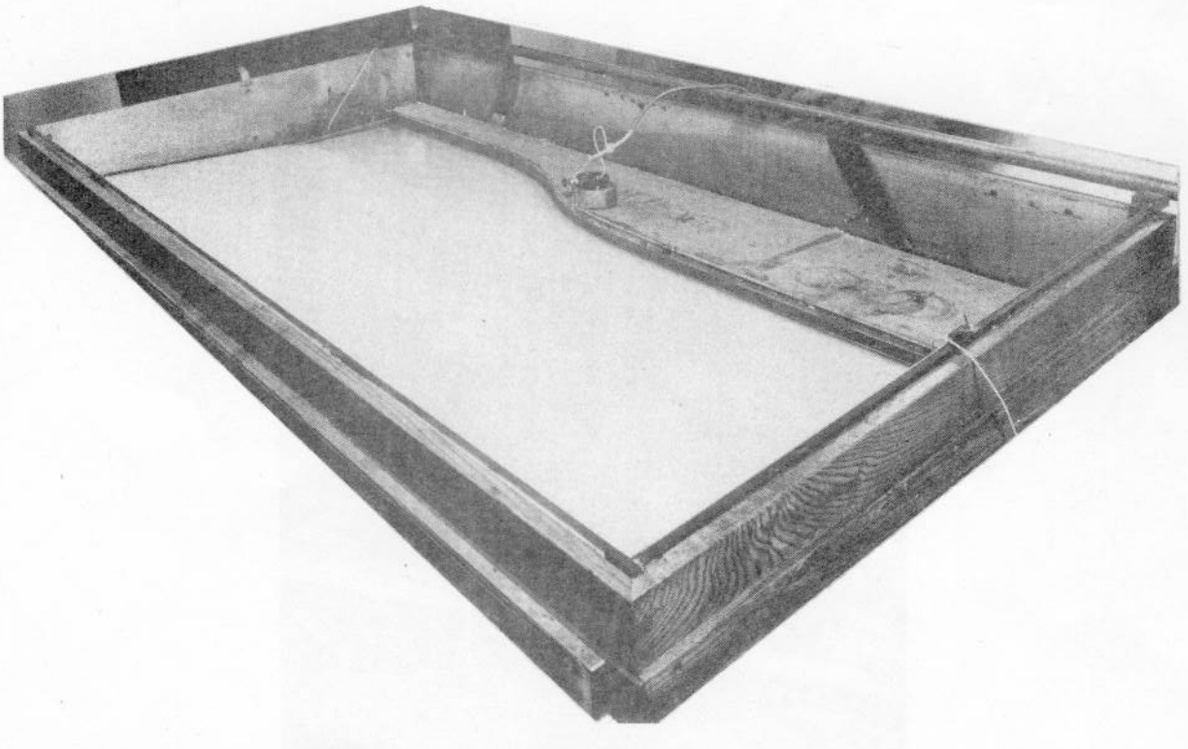

GENERAL VIEW OF TANK WITH WALL PROBE

FIG. 3

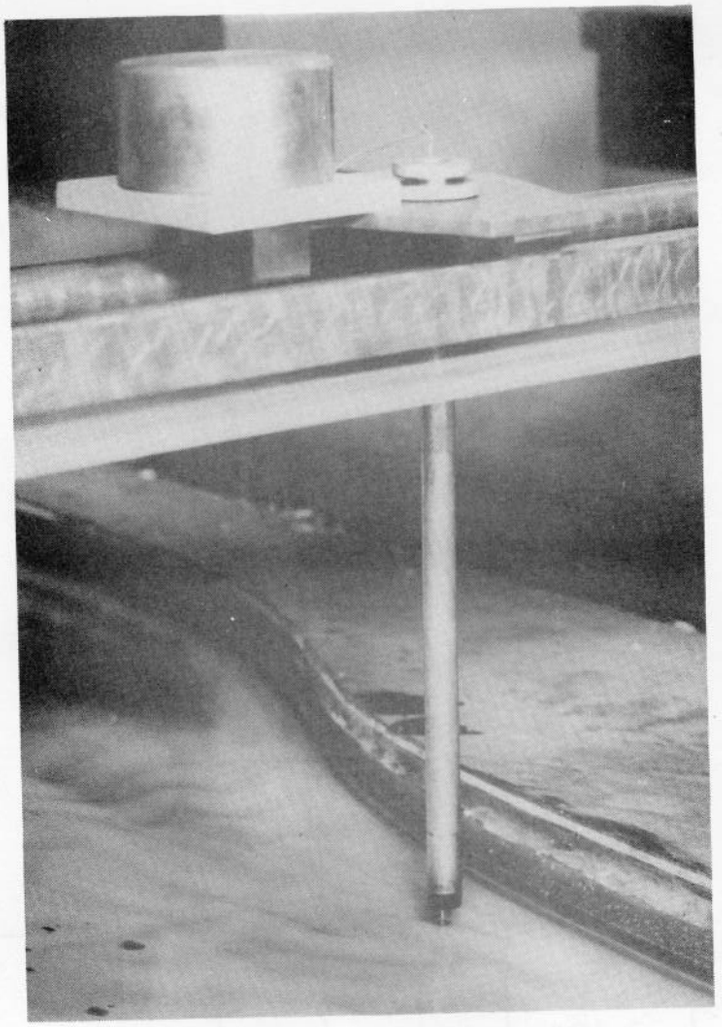

STANDARD PROBE

FIG. 4

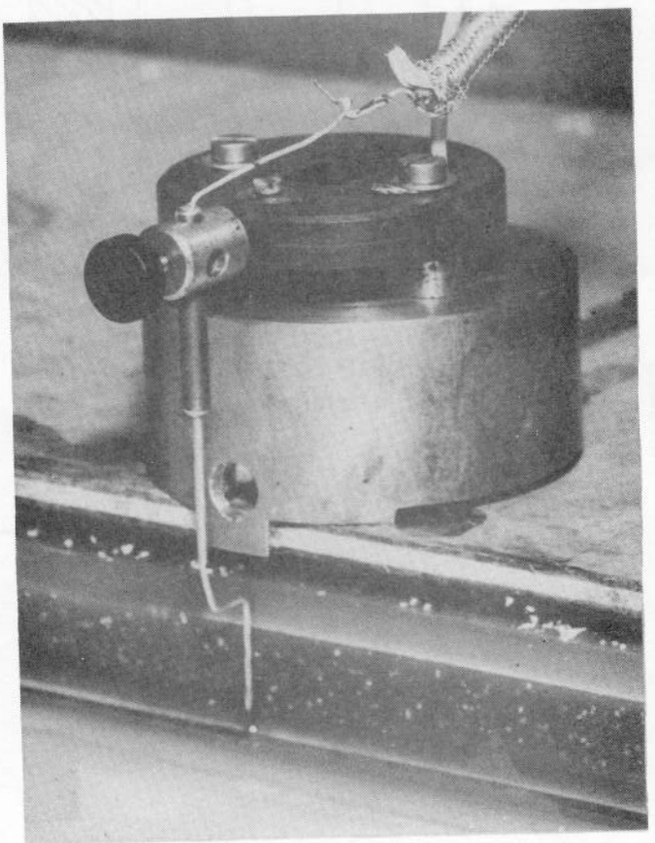

WALL PROBE

FIG. 5

FIG. 6.

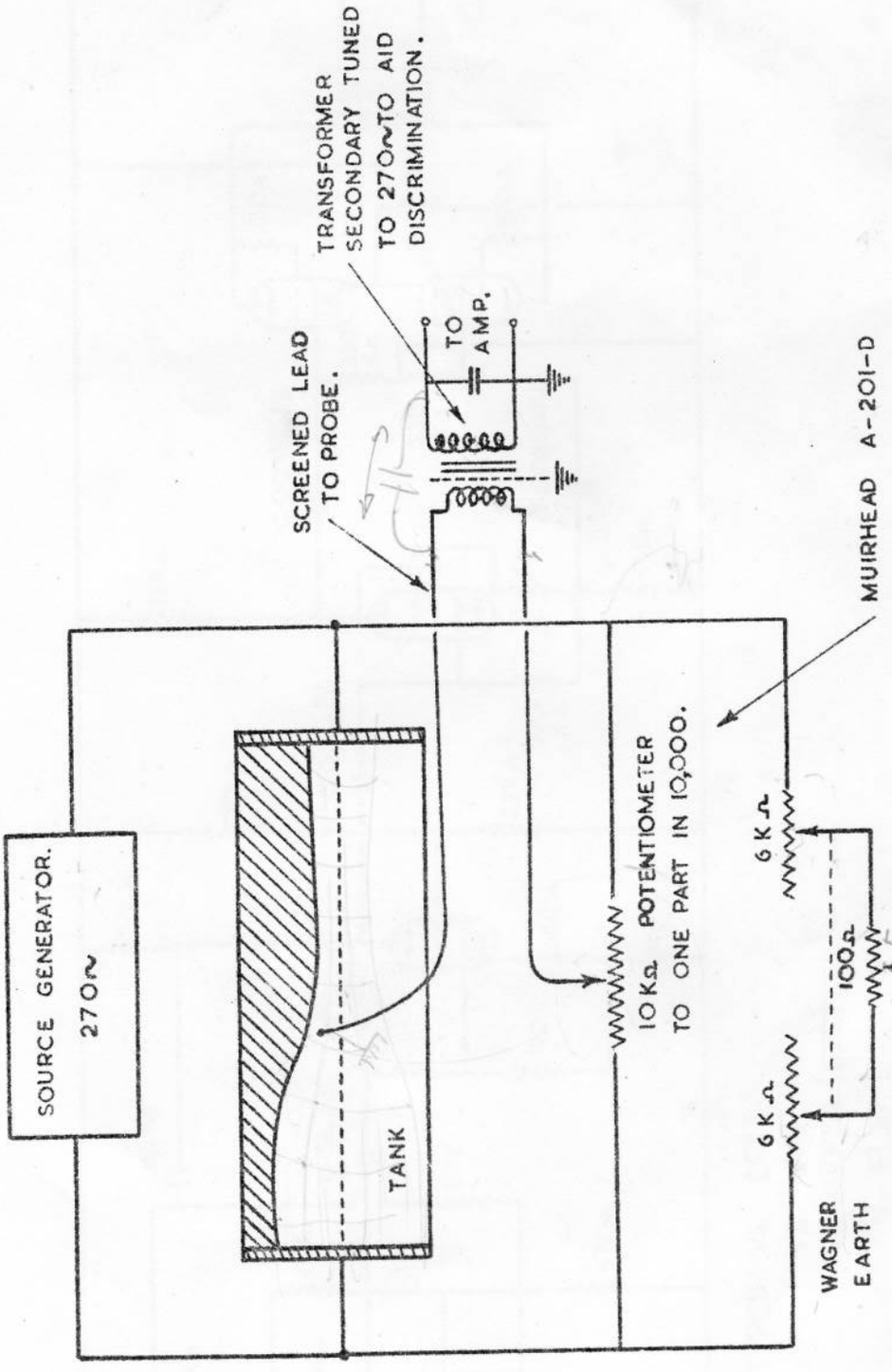

ARRANGEMENT OF TANK AND EQUIPMENT.

FIG. 7.

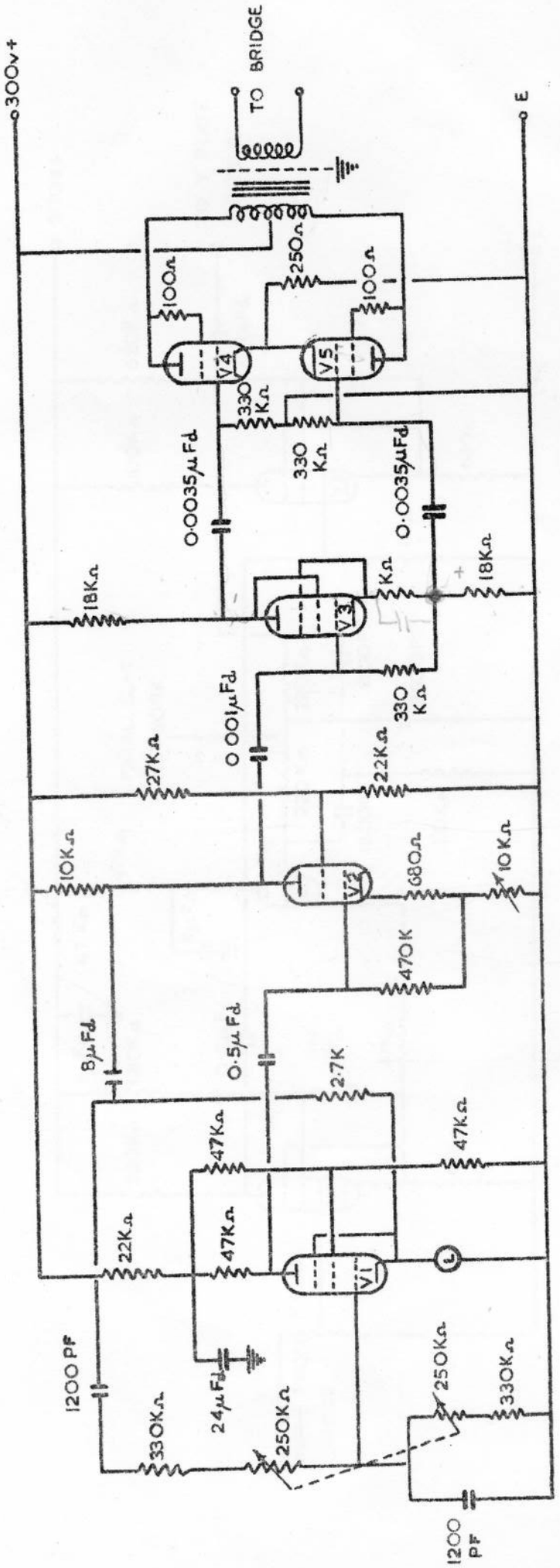

VALVE TYPES: V1. EF37.
V2. 6V6.
V3. EF36. (6J5.)
V4. EL37.
V5.
L 1SW. 230V. (PIGMY LAMP.)

WEIN BRIDGE OSCILLATOR AND POWER AMPLIFIER.

FIG. 8.

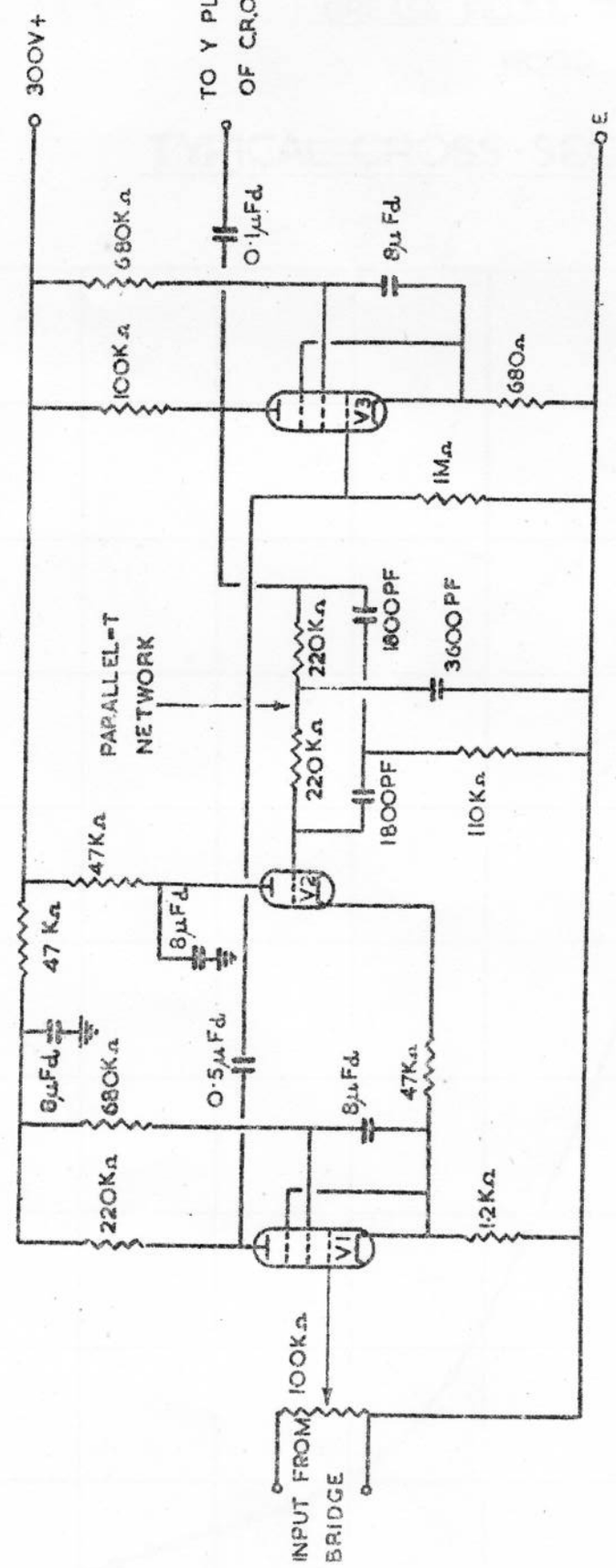

VALVE TYPES: V1. EF.37. GAIN = 83dB.
V2. 6J5.
V3. SP61.

HIGH GAIN AMPLIFIER.

COLLEGE OF AERONAUTICS
REPORT No. 46

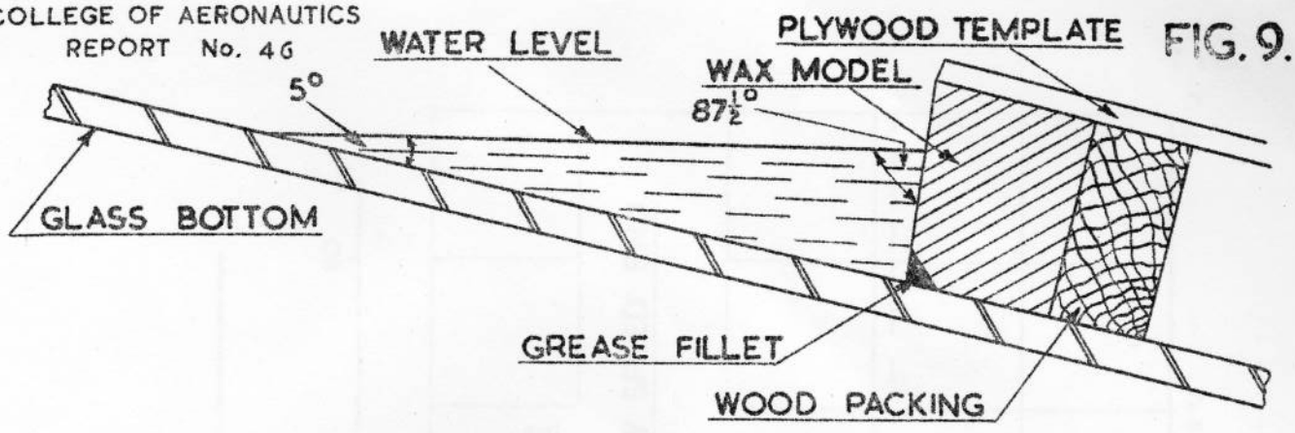

FIG. 9.

TYPICAL CROSS-SECTION.

FIG. 10.

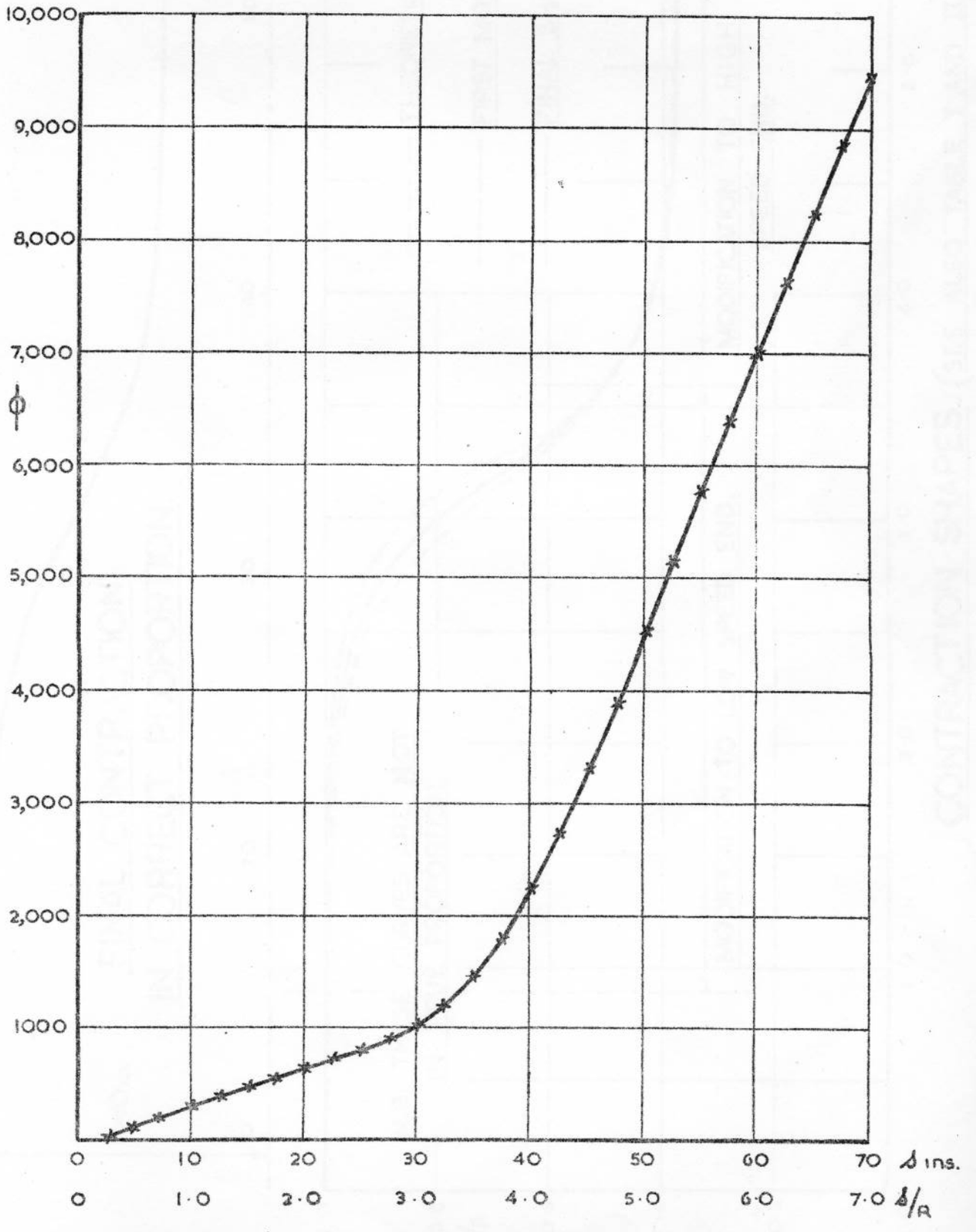

TYPICAL $\phi \sim \delta$ CURVE AS MEASURED.

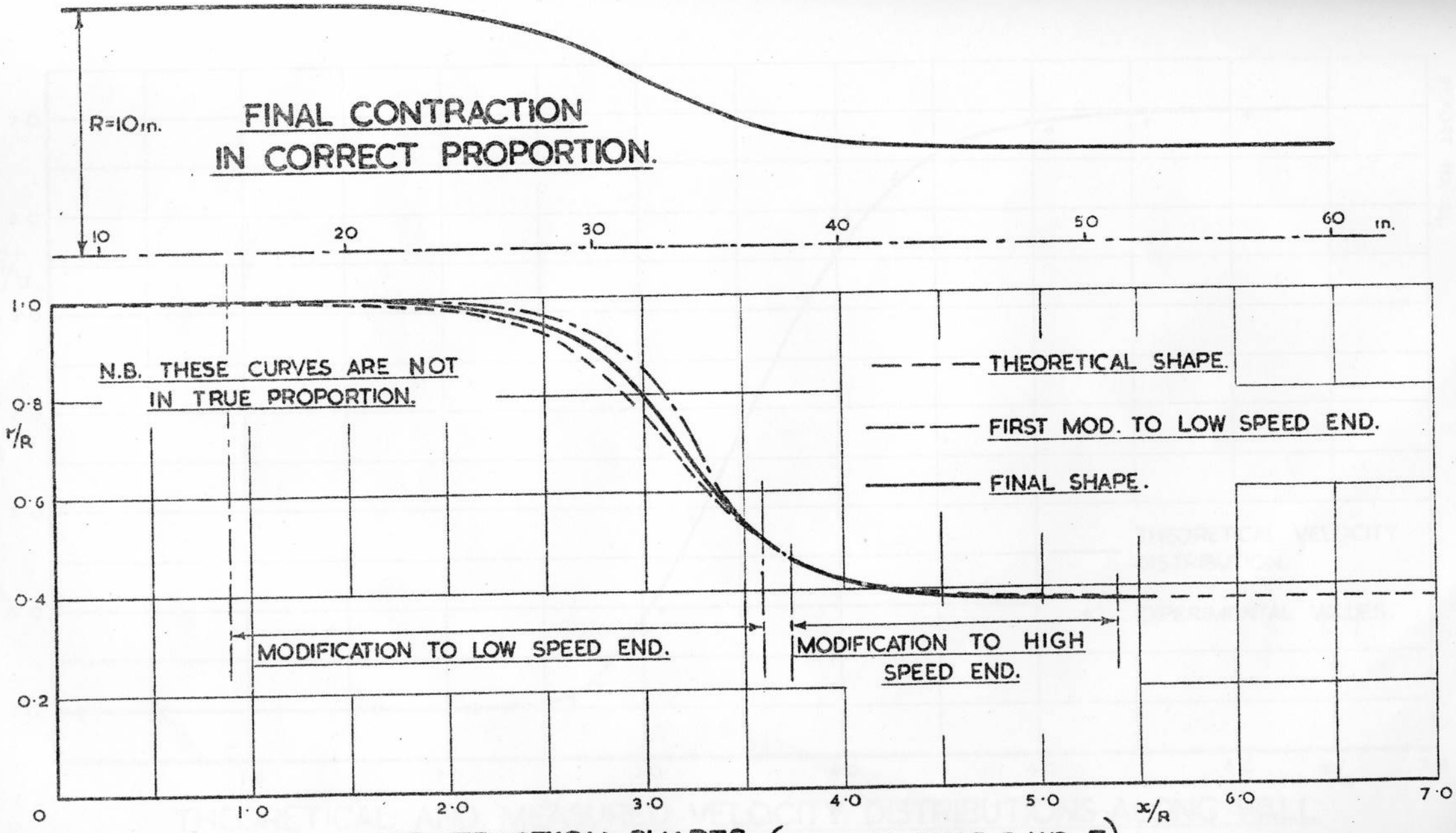

CONTRACTION SHAPES. (SEE ALSO TABLE I AND II).

FIG. 11.

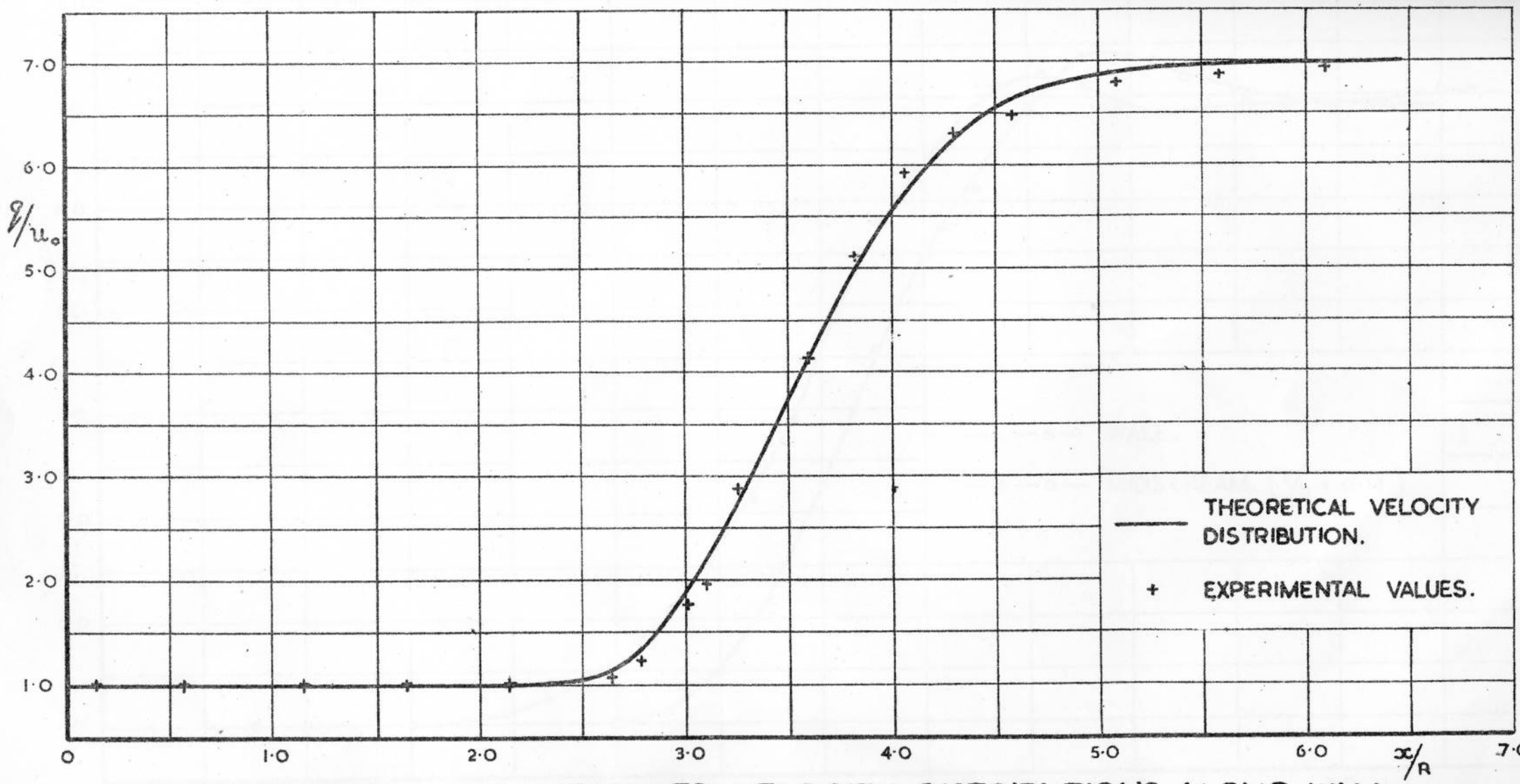

THEORETICAL AND MEASURED VELOCITY DISTRIBUTIONS ALONG WALL OF CONTRACTION.

FIG. 12.

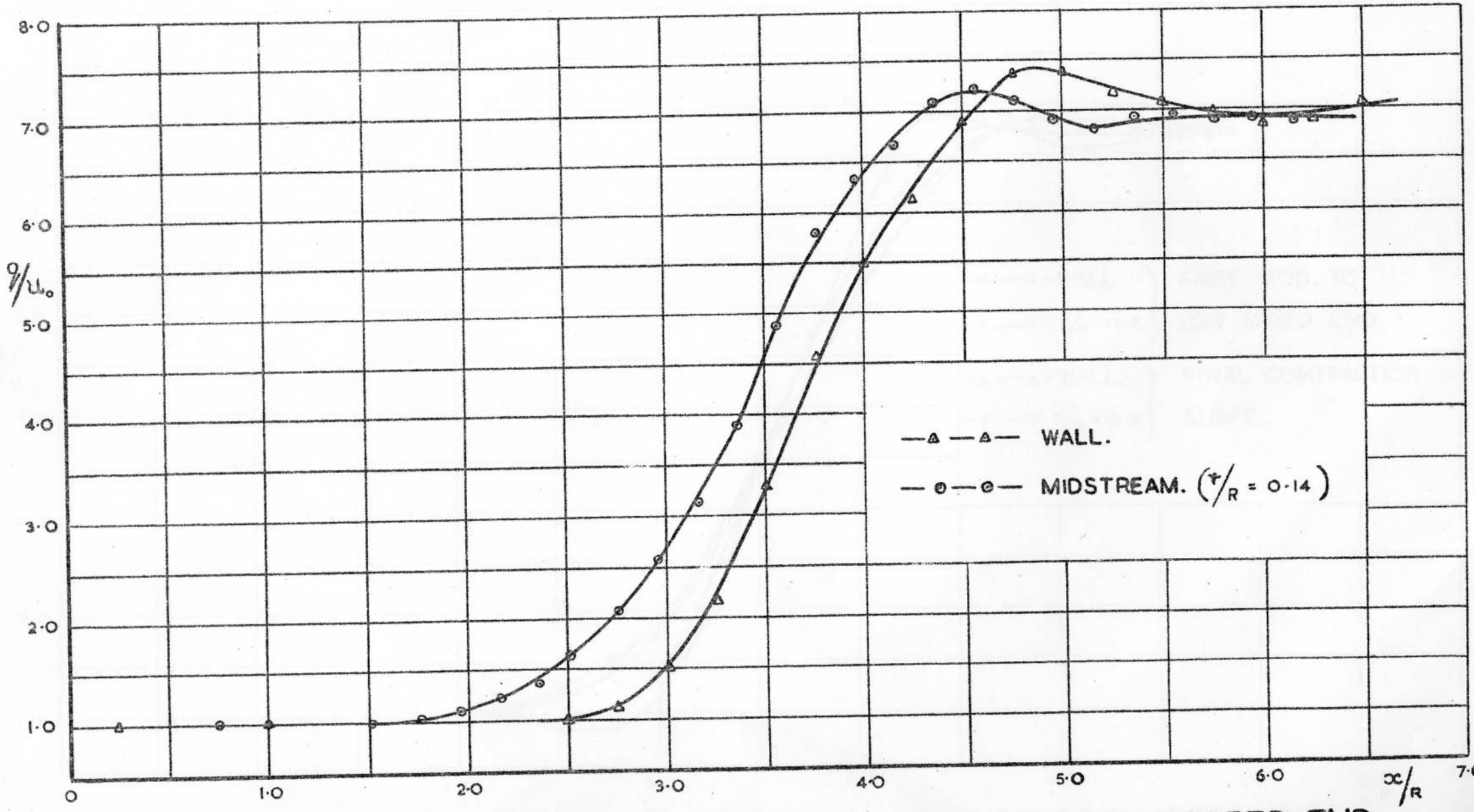

VELOCITY DISTRIBUTIONS AFTER MODIFICATIONS TO HIGH SPEED END.

FIG. 13.

FIG. 14.

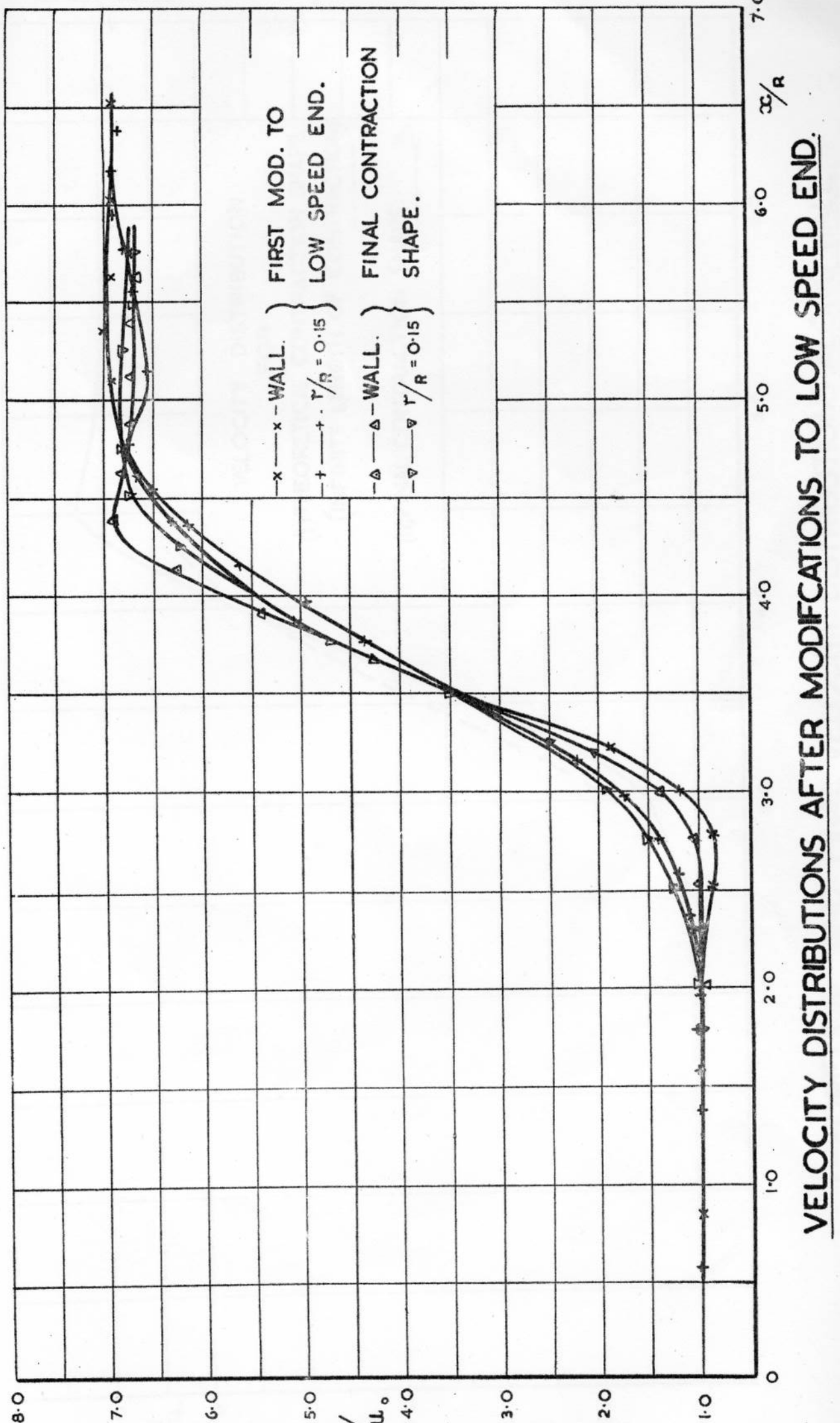

VELOCITY DISTRIBUTIONS AFTER MODIFCATIONS TO LOW SPEED END.

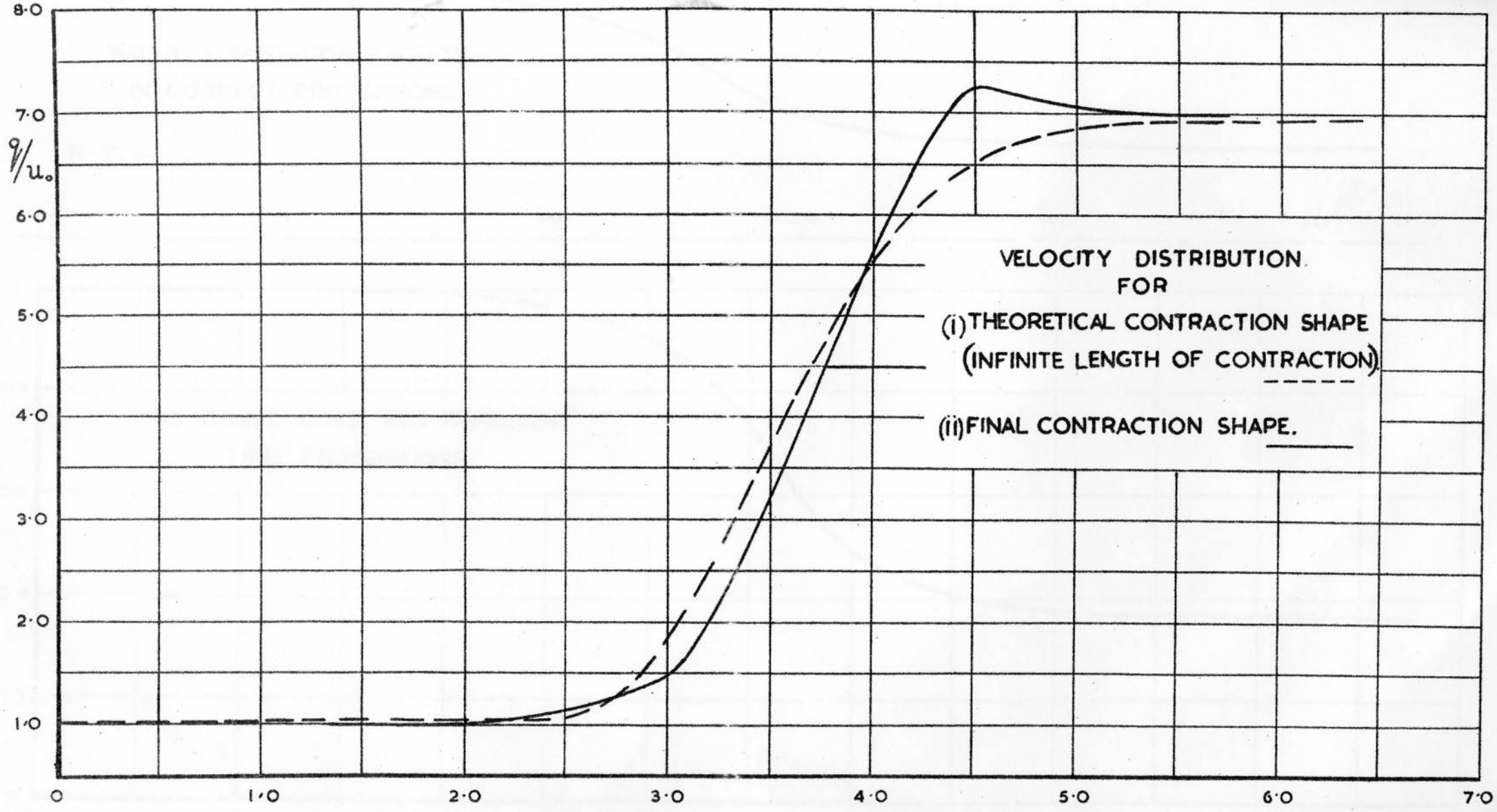

FIG. 15.

THEORETICAL AND FINAL VELOCITY DISTRIBUTIONS ALONG WALL.

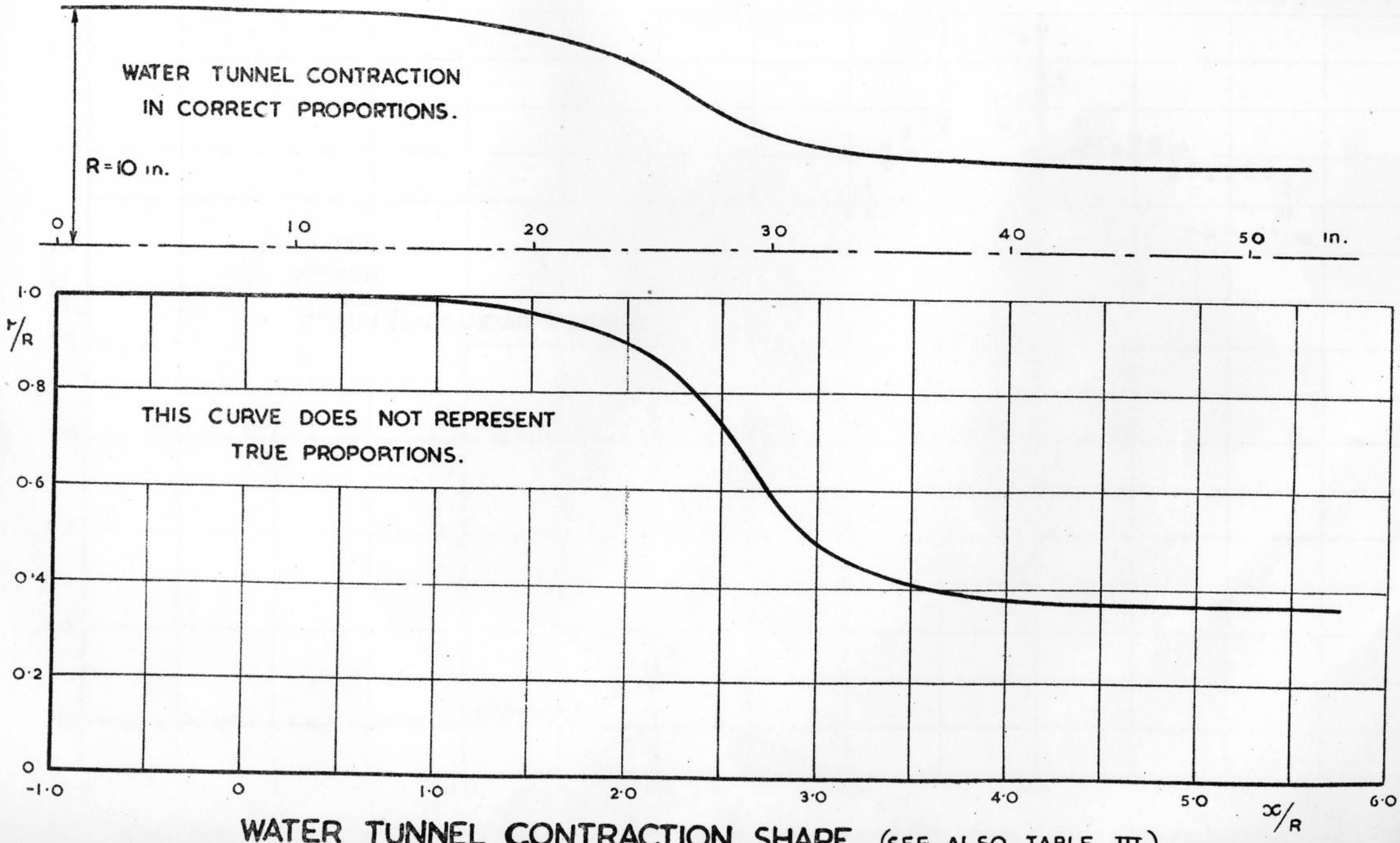

WATER TUNNEL CONTRACTION SHAPE. (SEE ALSO TABLE III).

FIG. 16.

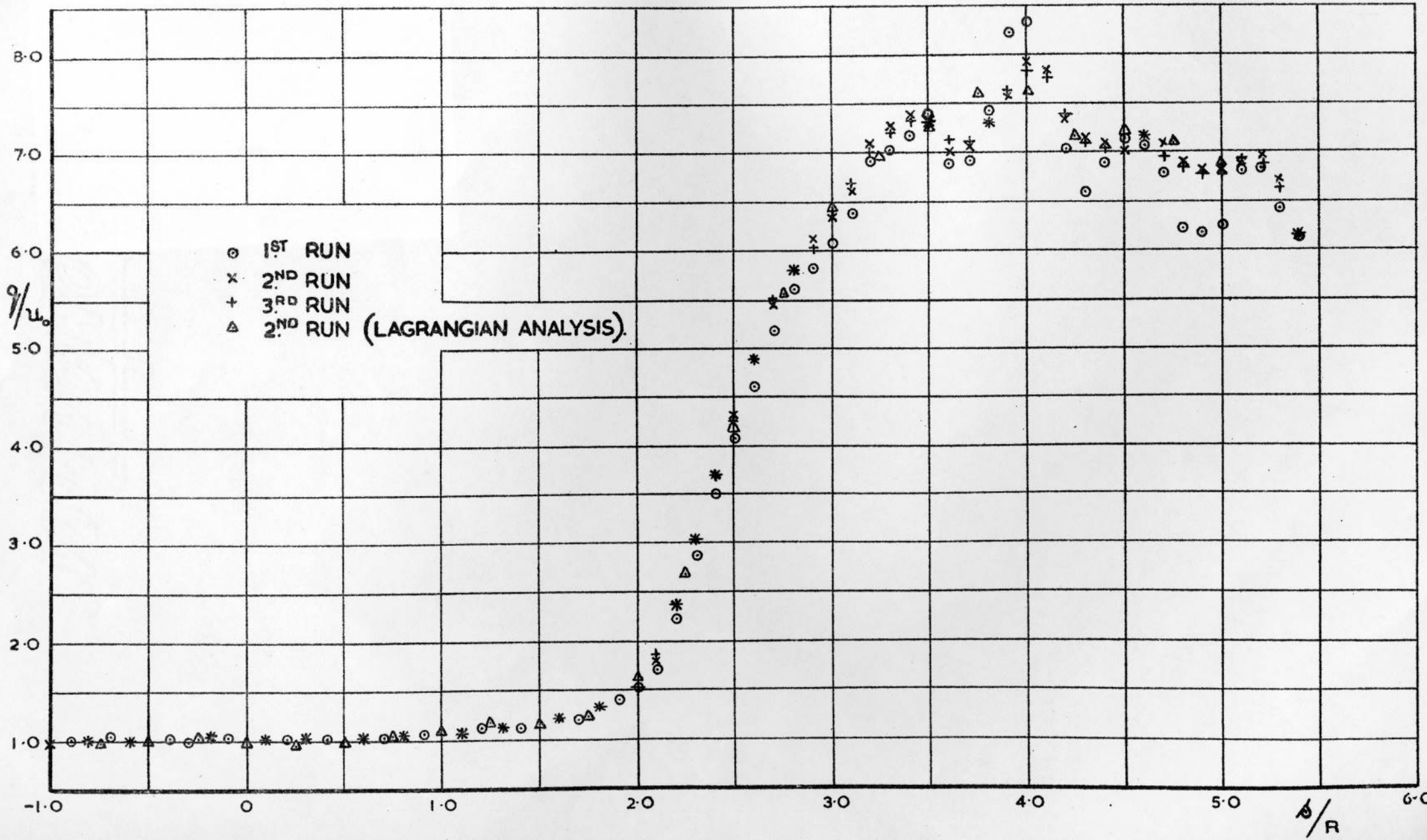

DISTRIBUTION OF VELOCITY ALONG WALL OF WATER TUNNEL CONTRACTION.

FIG. 17.